American Mineralogist, Volume 97, pages 1354–1365, 2012

Structural anisotropy and annealing-induced nanoscale atomic rearrangements in metamict titanite

Tobias Beirau,[1,*] Boriana Mihailova,[1] Galina Matveeva,[2] Ute Kolb,[2] Thomas Malcherek,[1] Lee A. Groat,[3] and Ulrich Bismayer[1]

[1]Department Geowissenschaften, Universität Hamburg, Grindelallee 48, D-20146 Hamburg, Germany
[2]Institut für Physikalische Chemie, Johannes Gutenberg-Universität Mainz, Welderweg 11, D-55099 Mainz, Germany
[3]Department of Earth and Ocean Sciences, University of British Columbia, Vancouver, British Columbia V6T 1Z4, Canada

Abstract

The structural state of metamict titanite was studied by Raman spectroscopy, complementary high-resolution transmission electron microscopy, and single-crystal X-ray diffraction. The results show that Raman scattering collected from metamict titanite is highly anisotropic, which is typical of single crystals. But surprisingly, the observed Raman-scattering dependence on the sample orientation is much more pronounced for heavily metamict than for weakly metamict titanite samples. These radiation-induced anisotropic effects are related to the specific atomic arrangements in metamict titanite. The Raman spectra collected in backscattering geometry from a plane nearly perpendicular to the chains of corner-sharing TiO_6 octahedra arise predominantly from phonon modes in crystalline nanoregions with radiation-induced defects, whereas the contribution of atomic vibrations in radiation-induced amorphous nanoregions is better pronounced in the Raman spectra collected from a plane containing TiO_6 chains. This difference provides a unique opportunity to study separately, the structural transformations of the crystalline and amorphous fractions in metamict titanite. The results show that the radiation-induced periodic faults in the crystalline matrix are related to the disturbance of SiO_4-TiO_6-SiO_4-TiO_6 rings comprising TiO_6 octahedra from different chains, whereas the radiation-induced amorphization is related to the partial change of Ti coordination from octahedral to pyramidal and/or tetrahedral, which in turn violates the Ti-O-Ti intrachain linkages. This indicates that the plane containing Si-O-Ti-O bond rings is less susceptible to a self-accumulation of radiation-induced defects resulting in the development of amorphous regions as compared to the perpendicular plane containing Ti-O bond chains. Sample-orientation-dependent Raman spectroscopy was further applied to annealed metamict titanite to give further insight into the temperature-driven recovery processes in the crystalline and amorphous nanoregions. Multistep annealing by 50 K for 2 h per step gradually suppresses the structural defects in the crystalline fraction as the improvement of the SiO_4-TiO_6 connectivity within planes nearly perpendicular to the TiO_6 chains reaches saturation near 900 K. The annealing-induced recrystallization of the radiation-induced amorphous nanoregions takes place in the temperature range between approximately 650 and 950 K, with a maximum near 750 K. Raman scattering shows that multistep annealing up to 1173 K is insufficient to recover the crystalline structure of the studied metamict titanite sample, which has an accumulated radiation dose of 1.2×10^{18} α-event/g.

Keywords: Metamict titanite, annealing, Raman spectroscopy, TEM

Introduction

Concerning the increasing amount of nuclear waste and the highly important question of permanent disposal (Ewing 2007a), it is of great importance to better understand the long-term influence of α-radiation on the structure of crystalline and amorphous materials. A frequently studied option for immobilization of actinides separated from former nuclear fuel is the encapsulation of the fuel in polycrystalline ceramics (Ewing 2007a; Farnan et al. 2007; Muller and Weber 2001; Weber et al. 1997, 1998). However, with time, the crystalline structure will be destroyed due to recoil processes associated with α-decay (Farnan et al. 2007; Muller and Weber 2001; Weber et al. 1997, 1998; Hawthorne et al. 1991; Ewing 2007b), which may lead to a release of the radioactive elements to the environment.

Metamict minerals possess structurally incorporated U and Th impurities and are characterized by a high degree of structural disorder consisting of the coexistence of defect-rich crystalline and amorphous nanoregions, caused by the radioactive α-decay of the embedded actinides. Thus, metamict minerals are ideal model systems for studying the behavior of actinide-bearing phases in specific geochemical environments and the structural stability of the host matrix over a geological timescale period (Ewing et al. 1988).

* E-mail: tobias.beirau@mineralogie.uni-hamburg.de

0003-004X/12/0809–1354$05.00/DOI: http://dx.doi.org/10.2138/am.2012.4024

The accessory mineral titanite with nominal chemical composition $CaTiSiO_5$ occurs in igneous and metamorphic rocks (Higgins and Ribbe 1976). In nature, Ca may be replaced by various impurities including the radionuclides U and Th. Due to the α-decay of these elements, the periodically ordered structure becomes partially destroyed and hence metamict (Hawthorne et al. 1991; Salje et al. 2011b). The structure of pure titanite consists of chains of corner-sharing TiO_6-octahedra, isolated SiO_4-tetrahedra and sevenfold-coordinated Ca^{2+} ions. The room-temperature phase of pure titanite is antipolar (space group $P2_1/c$) as a result of Ti^{4+}-cation off-center displacements, which are in the same direction within a single chain but opposite between two adjacent chains. On heating, pure titanite undergoes a space group $P2_1/c$-$C2/c$ phase transition at 487 K due to the loss of coupling of the Ti off-centered displacements from different chains and a subsequent isosymmetrical phase transition near 825 K, consisting of decoupling of the Ti off-centered displacements within a chain (Speer and Gibbs 1976; Taylor and Brown 1976; Zhang et al. 1995, 1997; Kek et al. 1997; Chrosch et al. 1997; Malcherek et al. 1999, 2001). Due to the existence of impurities and periodic faults in natural metamict titanite, the antipolar ordering is destroyed at room temperature and thus, at ambient conditions, the average crystal structure of metamict titanite is space group $C2/c$. The α-decay events in the structure result in the coexistence of crystalline and amorphous nanoregions as revealed by high-resolution transmission electron microscopy (HRTEM) (Lumpkin et al. 1991; Hawthorne et al. 1991). Mössbauer spectroscopic measurements show that the radiation-amorphized regions exhibit a significant degree of short-range order (Salje et al. 2011a). X-ray absorption spectroscopic (XAS) measurements of metamict titanite suggest increased disorder around the Ti positions with increasing degree of metamictization and a partial reduction of the Ti coordination from sixfold to five- and/or fourfold (Hawthorne et al. 1991; Farges 1997). On the basis of the results obtained by infrared spectroscopy (IRS), Zhang et al. (2002) also proposed that TiO_5 complexes exist in heavily metamict titanite.

Annealing experiments on metamict minerals can give further insights into the structural stability and the mesoscopic-scale atomic arrangements in radiation-damaged materials. Thermal annealing induces structural recovery (Hawthorne et al. 1991; Zhang et al. 2002; Paulmann et al. 2000; Beirau et al. 2010; Vance and Metson 1985), which, in general, consists of two processes: recrystallization of the radiation-amorphized nanoregions and suppression of the inherent structural defects in the crystalline fraction of the metamict sample. Infrared spectroscopy of titanite with various degree of metamictization clearly demonstrated the reduction of defects on the short-range length scale at elevated temperatures (Zhang et al. 2002). Synchrotron single-crystal X-ray diffraction (XRD) of heavily metamict titanite revealed a significant increase in the correlation length on the long range scale and a decrease in the unit-cell volume upon annealing at temperatures above 650 K (Paulmann et al. 2000; Beirau et al. 2010). A recent resonance-ultrasound-spectroscopy study of metamict titanite has shown that the annealing-induced annihilation of point defects in the crystalline regions and recrystallization of amorphous regions occur between 573 and 923 K, which surprisingly leads to a softening of the shear moduli (Salje et al. 2011b).

Our previous Raman spectroscopic experiments (Beirau et al. 2010) involving several metamict titanite samples revealed a strong structural anisotropy that is more pronounced for titanite with a higher degree of metamictization. The long-range coherence seems to be less affected within one plane, whereas amorphization is more prominent in the near perpendicular plane. The objective of this study is to clarify the reason for this structural anisotropy enhanced in radiation-damaged titanite and to elucidate the structural transformations that take place in metamict titanite during annealing on the mesoscopic length scale, using sample-orientation-dependent Raman spectroscopy as well as complementary transmission-electron microscopy and single-crystal XRD.

Experimental methods

We have chosen to study metamict titanite from the collection of the Royal Ontario Museum (ROM), Department of Mineralogy, Toronto, Ontario, Canada, by Raman spectroscopy. The samples have been thoroughly analyzed by other research groups using various methods, including electron microprobe analysis (EMPA), X-ray diffraction (XRD), Mössbauer spectroscopy, etc. (Hawthorne et al. 1991; Salje et al. 2011a, 2012). The main characteristics of the samples are summarized in Table 1. It should be noted that heavily metamict titanite is rather inhomogeneous and this is probably the reason for the deviation in the U and Th content of titanite from the Cardiff locality (ROM catalog number M28696) reported in different papers (Hawthorne et al. 1991; Chrosch et al. 1998; Salje et al. 2012). Since the concentration of U in sample M28173 given by Hawthorne et al. (1991) was surprisingly high (2620 ppm), we measured this sample by EMPA with a Cameca microbeam SX100 SEM system. Operating conditions were a 15 kV accelerating voltage, 40 nA beam current, a beam spot diameter on the same surface approximately 1 μm averaged over 10 points. The analyses indeed revealed a U content that is lower than that for sample M28696 (see Table 1) and thus better matches the index of structural damage estimated from XRD and infrared spectroscopic (IRS) analysis.

We have chosen metamict titanite with an ROM catalog number E2335 as a model metamict titanite to study the annealing-induced structural alteration because this sample exhibits phase homogeneity on the length scale of XRD sensitivity and a relatively low degree of chemical impurities (Salje et al. 2011b; Hawthorne et al. 1991). The fraction of the amorphized material in sample E2335

Table 1. Chemical and structural characteristics of the metamict samples studied

ROM catalog number	U (ppm)	Th (ppm)	Reference	Time (Ma)	Reference	Damage index*		Dose† (10^{18} α-event/g)
						XRD	IR	
M28658	22	1	Hawthorne et al. (1991)	2502‡	Tucker et al. (1999)	3	3	0.2§
E2335	135 ± 24	764 ± 141	Salje et al. (2012)	1086	Salje et al. (2012)	9	8	1.19 ± 0.22
M28173	305 ± 100	410 ± 110	Our data	1000‡	Vance and Metson (1985)	8	9	1.4 ± 0.4
M28696	473 ± 64	498 ± 56	Salje et al. (2012)	1035	Salje et al. (2012)	10	10	2.17 ± 0.29

* After Hawthorne et al. (1991).
† Calculated after Nasdala et al. (2001); the uncertainties are calculated from the uncertainties in the U and Th contents.
‡ The time used to calculate the dose was approximated with the age of the rocks from the same type and locality given in the corresponding papers.
§ No available literature data about the uncertainties in the U and Th contents.

has been determined to be 0.24 (Salje et al. 2011a). The crystals are black to black-brown and become brownish and transparent after annealing.

Multistep annealing of the metamict titanite sample E2335 was carried out in a Thermo-Scientific Laboratory Chamber Furnace K114. The heating temperature was controlled by an AHLBORN THERM 2420 temperature-measuring device equipped with a NiCr-Ni thermocouple, which ensures a thermal stability of ±2 K. The sample was annealed at temperatures in the range 423–1173 K with steps of 50 K. The annealing time at each step was 2 h. The heating period before each annealing step was approximately 35 min. After each annealing step the sample was cooled to room temperature and a Raman spectrum was recorded.

Raman spectroscopic measurements were performed on polished plane-parallel specimens cut in random orientation, using a Horiba Jobin-Yvon T64000 triple monochromator system operating in a subtractive regime and equipped with a liquid N_2-cooled charge-coupled device (CCD) detector and an Olympus BH41 microscope. Spectra were collected in back-scattering geometry without analyzer of the scattered light, using the 514.5 nm line of an Ar^+-ion laser and a long-working distance objective with magnification 50×. The diameter of the laser spot on the sample surface was approximately 2 µm. The laser power surface density delivered to the sample was 1.5 kW/mm^2, as it was verified that such a power density does not change the sample due to undesired overheating. The achieved instrumental spectral resolution was ~2 cm^{-1}. Since our Raman lab is equipped with an air conditioner ensuring stability of the room temperature and consequently, thermal stability of the gratings, there are no variations of peak positions related to a plausible subtle thermal expansion of the dispersive element. The Raman spectroscopic system was always calibrated to the position of the Si peak at 520.5 cm^{-1} with a precision of ±0.35 cm^{-1}. The spectra were measured in the same spectral range, i.e., the gratings were always positioned in the same manner to avoid any inaccuracy in the peak positions related to the slight non-linearity of the signal on the CCD detector. Therefore, the achieved experimental precision in determining the peak positions was ~0.5 cm^{-1}. For each sample, Raman spectra from several points (approximately 10 per sample) were collected to check the reproducibility of the spectra, i.e., the homogeneity of the samples with respect to the Raman scattering signals. It was found that under the experimental conditions, the spatial variations of the Raman spectra were negligible, if the orientation of the sample were kept constant. This means that the efficient scattering volume (on the order of cubic micrometers) is indeed much larger than the expected nanometric length scale of structural inhomogeneity in metamict titanite. Additionally, we conducted measurements with the 488.0 nm line of the Ar^+-ion laser to identify possible photoluminescence signals.

Raman spectra were measured after each annealing step from two different orientations of the metamict titanite sample (E2335) with respect to the directions of the incident-light propagation and polarization. As in Raman spectra of non-annealed samples, the Raman scattering collected from different spatial areas of sample E2335 (after the subsequent annealing step) showed good reproducibility. The spectra were recorded from the same region of the sample, with an uncertainty of ~20 µm. The two sample orientations are designated as orientations 1 and 2, following the nomenclature in Beirau et al. (2010). The two orientations are approximately perpendicular to each other. The Raman spectrum of metamict titanite with a damage index 10 collected in orientation 1 corresponds most closely to the spectrum of well-crystalline titanite, whereas the Raman spectrum collected in orientation 2 is substantially different (Beirau et al. 2010).

The measured spectra were reduced by the Bose-Einstein occupation factor $\{I_{reduced} = I_{measured}/[n(\omega,T) + 1],\ n(\omega,T) = 1/(e^{\hbar\omega/kT} - 1)\}$ and fitted by Lorentzian functions using the software package Origin 8.5, to determine the peak positions, full-widths at half maximum (FWHM), and integrated intensities. The spectra measured after each annealing step were fitted with the same number of Lorentzian functions used for non-annealed metamict titanite and no constraints were applied on the peak parameters when fitting.

The crystallographic orientation of the sample and the Miller indices of the faces were obtained using a Nonius Kappa CCD single-crystal diffractometer with Mo$K\alpha$ radiation. Indexing of diffraction spots was performed using Denzo (Otwinowski and Minor 1997). The obtained unit-cell setting of titanite corresponds to that described by Hawthorne et al. (1991).

The intrinsic nanometer-scale structural inhomogeneity of the studied metamict titanite was probed by transmission electron microscopy (TEM). Pieces of random orientation and size between 0.1 and 1 µm were dispersed in ethanol and mounted on a carbon-coated copper grid using an ultrasonic sprayer. TEM experiments were performed with an FEI TECNAI F30 microscope equipped with a Super-twin lens, operating at 300 kV using a scanning TEM unit with a HAADF detector and a 1 × 1 K slow scan CCD camera. The measurements were conducted using a double tilt halter at room temperature.

Results and discussion

Transmission electron microscopy

Many submicrometer particles of E2335 were examined by scanning TEM and showed monocrystalline diffraction patterns (see Fig. 1a). TEM images were used for more detailed examination of randomly chosen crystals of sample E2335. As can be seen in Figure 1b, the crystals exhibit structural inhomogeneities and variations in thickness. However, high-resolution (HR) TEM images obtained from different peripheral parts of this crystal provided identical fast Fourier transform (FFT) patterns (see the inset in Fig. 1b). Coexisting nanoregions with crystalline fringes and lack of periodicity are clearly seen in the HRTEM images (Fig. 2a). Under higher magnification, periodic faults inside the crystalline nanoregions are also revealed (Fig. 2b). The size and fraction of amorphous regions vary from area to area and hence, HRTEM alone cannot provide a statistically relevant estimation of the proportion of amorphous regions in the sample.

Raman spectroscopy

Group-theory analysis of pure titanite. First-order infrared absorption and Raman scattering spectra of pure titanite can be described by the corresponding optically active irreducible representations at the center of the Brillouin zone (Kroumova et al. 2003). The Γ-point phonon modes associated with the occupied Wyckoff positions in the two titanite phases with space groups $C2/c$ and $P2_1/c$ are given in Table 2. Experimentally, 31 Raman signals were resolved in the spectra of synthetic single-crystal titanite (see Fig. 3), which is less than the number of expected Raman-active modes for the room temperature phase space group $P2_1/c$ ($24A_g + 24B_g = 48$ in total), but more than the Raman-active modes allowed in space group $C2/c$ ($9A_g + 12B_g = 21$ in total). The smaller number of experimentally observed Raman peaks than that predicted by group theory for space group $P2_1/c$ is most likely due to the weak intensities of some modes and/or overlapping of peaks generated from modes of different symmetry but involving the same types of atomic vibrations in terms of stretching, bending, etc.

It should be noted that Raman spectra collected with a dispersive spectrometer and a linearly polarized laser were always partially polarized, even when no analyzer was used on the scattered light, due to the inherent transmission efficiency of the gratings. Therefore, some discussion about the orientation dependence of the Raman scattering intensities for pure single-crystal titanite is required. For our experimental setup, the strongest contribution to the Raman spectra comes from the scattered light, which has a polarization $\mathbf{E}_s$ parallel to the polarization of the incident light $\mathbf{E}_i$. The matrix representations of the Raman polarizability tensors for A_g and B_g modes in a monoclinic system with unique axis b are

$$A_g: \begin{pmatrix} a & 0 & d \\ 0 & b & 0 \\ d & 0 & c \end{pmatrix} \text{ and } \quad B_g: \begin{pmatrix} 0 & e & 0 \\ e & 0 & f \\ 0 & f & 0 \end{pmatrix}.$$

Hence, when the monoclinic binary axis coincides with the polarization of the incident light $\mathbf{E}_i$, the parallel-polarized Raman spectra ($\mathbf{E}_i \parallel \mathbf{E}_s$) are generated from the A_g modes, whereas the

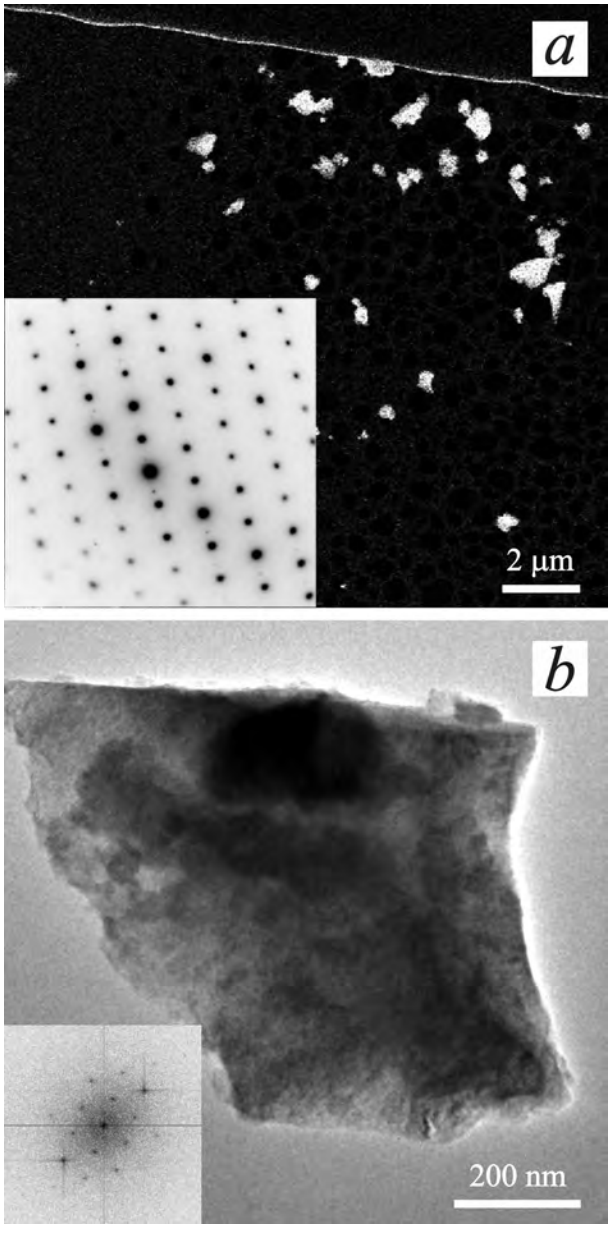

FIGURE 1. Typical scanning TEM image (**a**) and electron diffraction pattern (inset in **a**) of sample E2335 as well as TEM image of a single, randomly chosen E2335 particle (**b**) and the calculated FFT pattern (inset in **b**) for the peripheral part, which corresponds to the crystallographic [1$\bar{1}$1] zone.

cross-polarized spectra ($\mathbf{E}_i \perp \mathbf{E}_s$) result from the B_g modes. In the case of a randomly oriented sample with respect to the scattering geometry, all components of the polarizability tensors for both A_g and B_g modes are nonzero, following the transformation rules for a second-rank tensor upon three successive rotations describing the orientation of the sample with respect to the special case $b \parallel \mathbf{E}_i$. Thus, both A_g and B_g modes contribute to the parallel as well as to the cross-polarized Raman spectrum and the weight coefficients of the polarizability tensor components are complex functions of the angles of rotation. Therefore, the

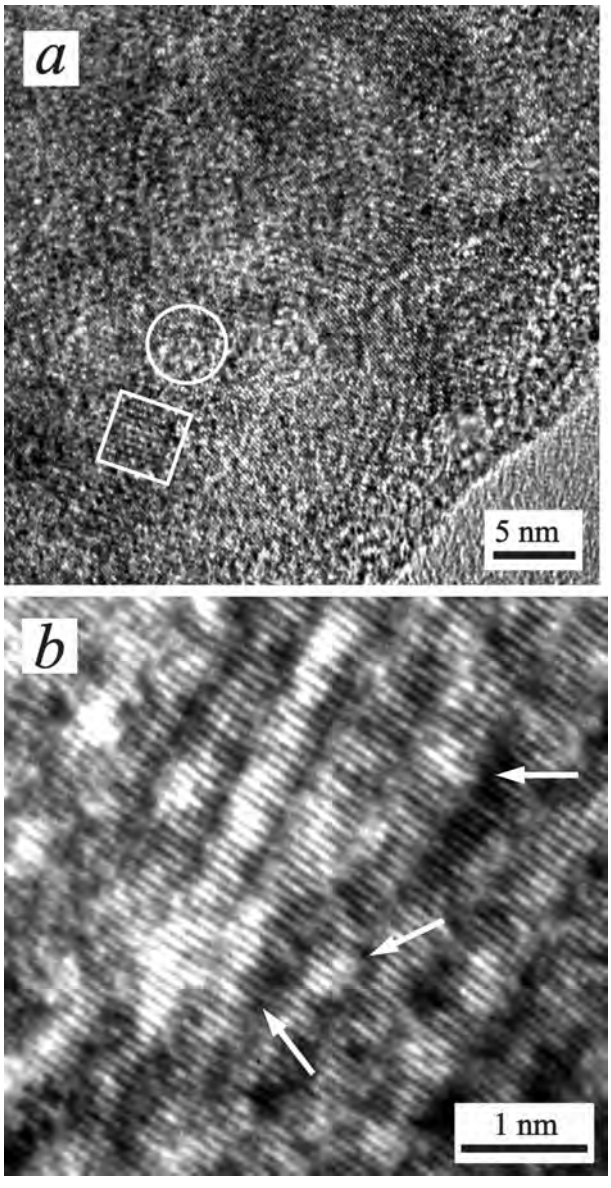

FIGURE 2. HRTEM images obtained from different parts of the crystal shown in Figure 1b. The white rectangle and circle in **a** mark crystalline and amorphous nanoregions, respectively. The white arrows in **b** point to edge dislocations.

TABLE 2. Site-symmetry analysis of the allowed Brillouin-zone-center phonon modes in pure titanite; R stands for Raman-active, IR for infrared-active

Space group $P2_1/c$	Space group $C2/c$
Ca (4*e*): $3A_g + 3A_u + 3B_g + 3B_u$	Ca (4*e*): $A_g + A_u + 2B_g + 2B_u$
Ti (4*e*): $3A_g + 3A_u + 3B_g + 3B_u$	Ti (4*b*): $3A_u + 3B_u$
Si (4*e*): $3A_g + 3A_u + 3B_g + 3B_u$	Si (4*e*): $A_g + A_u + 2B_g + 2B_u$
O1 (4*e*): $3A_g + 3A_u + 3B_g + 3B_u$	O1 (4*e*): $A_g + A_u + 2B_g + 2B_u$
O2 (4*e*): $3A_g + 3A_u + 3B_g + 3B_u$	O2 (8*f*): $3A_g + 3A_u + 3B_g + 3B_u$
O3 (4*e*): $3A_g + 3A_u + 3B_g + 3B_u$	O3 (8*f*): $3A_g + 3A_u + 3B_g + 3B_u$
O4 (4*e*): $3A_g + 3A_u + 3B_g + 3B_u$	
O5 (4*e*): $3A_g + 3A_u + 3B_g + 3B_u$	
$\Gamma_{optic} = 24A_g$ (R) + $23A_u$ (IR) + $24B_g$ (R) + $22B_u$ (IR)	$\Gamma_{optic} = 9A_g$ (R) + $11A_u$ (IR) + $12B_g$ (R) + $13B_u$ (IR)
$\Gamma_{acoustic} = A_u + 2B_u$	$\Gamma_{acoustic} = A_u + 2B_u$

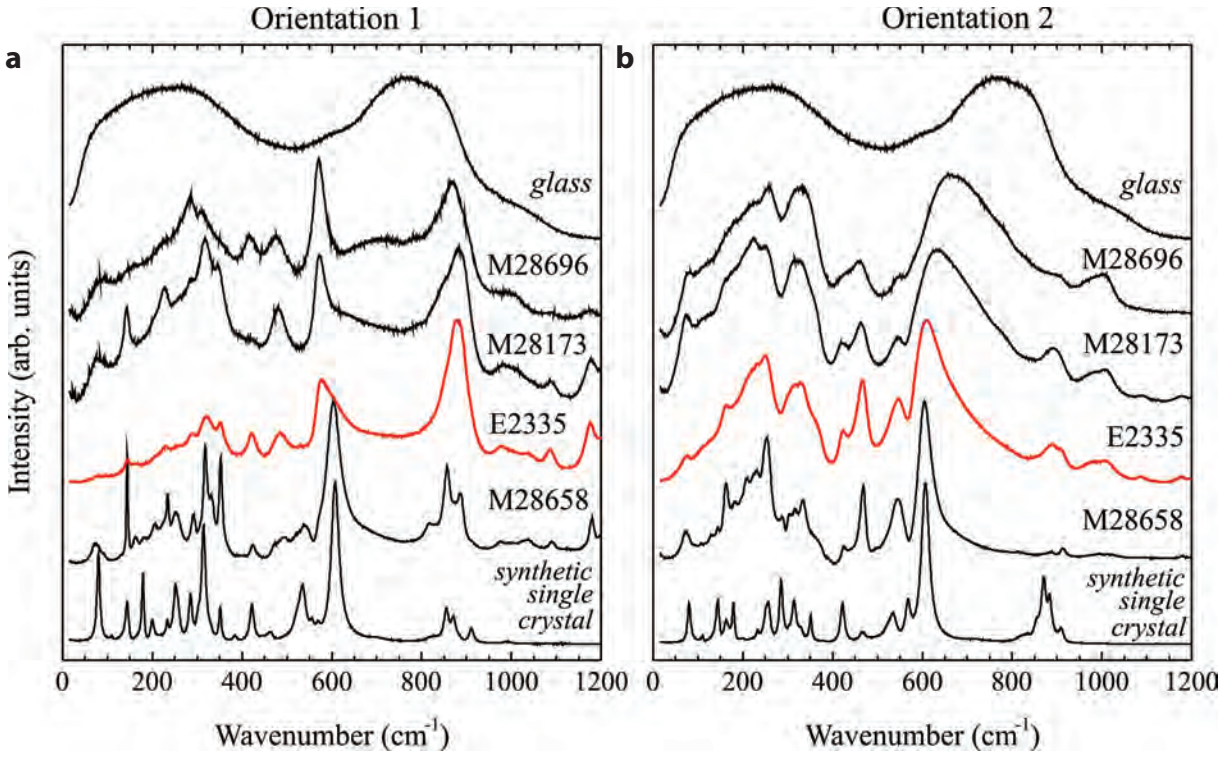

FIGURE 3. Raman spectra of sample E2335 in orientation 1 (**a**) and orientation 2 (**b**) compared with the corresponding Raman spectra of metamict titanite samples with different degree of metamictization (see Table 1). The signals near 1180, 1090, and 1045 cm^{-1} are photoluminescence peaks. For sample E2335, the band near 880 cm^{-1} in orientation 1 results from overlapping Raman and photoluminescence signals. The Raman spectra of synthetic single-crystal titanite and amorphous titanite obtained by a rapid cooling of melted synthetic polycrystalline titanite are also given for comparison. (Color online.)

Raman scattering intensities in the spectra collected from single crystals of titanite are expected to be orientation dependent. This dependence should be strong if the difference between the initial tensor components (*a*, *b*, *c*, *d*, *e*, and *f*) is large. The experimentally observed Raman scattering of synthetic single-crystal titanite exhibits orientational dependence, but the differences in the intensities are not very large. As an example, Figure 3 depicts spectra of synthetic single-crystal titanite measured when the monoclinic binary axis was approximately perpendicular to the propagation of the incident light (orientation 1) and when the binary axis was more or less parallel to the propagation of the incident light (orientation 2). As illustrated, the main features of the spectra measured in the two orientations are similar and, in particular, the scattering in the range 600–800 cm^{-1} is identical.

Anisotropy of Raman scattering related to the radiation-induced structural damage. A sketch of the orientation of the sample E2335 specimen with respect to the direction of the propagation, $\mathbf{k}_i$, and the polarization vector, $\mathbf{E}_i$, of the incident light is provided in Figure 4. Orientation 1 corresponds to the case in which $\mathbf{k}_i$ is perpendicular to the crystallographic plane $(\bar{2}\,\bar{2}3)$ (Miller indices refer to space group *C*2/*c*); $\mathbf{E}_i$ is perpendicular to $(\bar{2}41)$. In orientation 2, the incident light propagates in a direction perpendicular to the crystallographic plane $(\bar{2}41)$, whereas the polarization $\mathbf{E}_i$ is perpendicular to $(\bar{2}\,\bar{2}3)$. It should be noted that, for both scattering geometries, the in-plane rotation of the sample has little effect on the spectrum profile.

The Raman spectra collected from sample E2335 are compared with the spectra of other titanite samples in Figure 3. The spectra of all radiation-damaged titanite samples could be successfully fitted with the same number of Lorentzian functions, which however, differ from the number of functions used for synthetic titanite due to two reasons: (1) the appearance of new peaks in the range 600–900 cm^{-1} as a result of the symmetry breakdown and development of non-crystalline regions; (2) the fact that some of the weak peaks observed in the spectrum of crystalline titanite could not be resolved in the spectra of metamict samples and hence, the corresponding Lorentzian functions were skipped while fitting the spectra.

Based on the overall Raman-peak broadening, which is indicative of structural defects, one can suggest that the damage index of sample E2335 is higher than that of sample M28658 but lower than that of sample M28173. Thus, the Raman-scattering data better match the IRS criterion rather than the XRD criterion as defined by Hawthorne et al. (1991). The peak positions and FWHMs apparently correlate with the accumulated radiation doses. For example, in Figure 5 the FWHM of the peak near 465 cm^{-1} measured in orientation 2 is plotted against the α-radiation dose. This peak is particularly suitable for estimating the degree of metamictization because: (1) it arises from the SiO_4 bending mode (Heyns et al. 2000), which means that the peak parameters

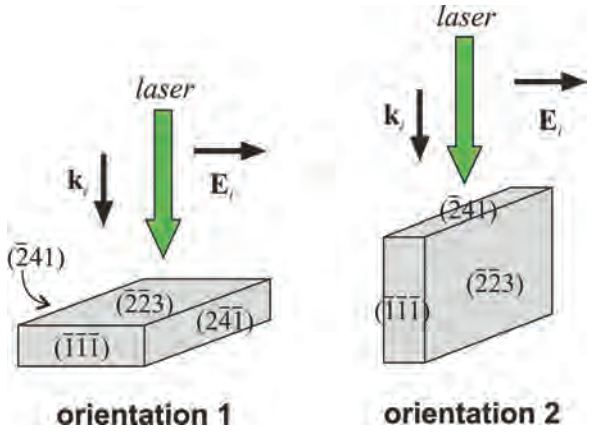

FIGURE 4. Sketch of the crystal orientation during the Raman-scattering measurements; $\mathbf{k}_i$ denotes the direction of the propagation of the incident laser light, whereas $\mathbf{E}_i$ is the polarization of the laser. Miller indices are given for space group *C*2/*c*. No analyzer was used in the experiments. In-plane rotation of the sample had little effect on the spectrum profile, indicating that the difference in the Raman scattering collected in orientation 1 and orientation 2 is related to quasi-planar structural species in the plane parallel to $\mathbf{E}_i$, rather than to quasi-linear structural species along the direction of $\mathbf{E}_i$. (Color online.)

are least affected by the presence of chemical impurities which commonly substitute for Ti and Ca, and; (2) for all metamict samples it is relatively well-separated, ensuring small errors in the peak parameters obtained by fitting. However, many well-characterized samples should be analyzed to establish a calibration curve and one should keep in mind that, in general, the Raman peak positions and FWHMs may also be influenced by the geologic history of the sample (Geisler and Pidgeon 2002).

Similar to other heavily metamict titanite samples with a damage index ≥8 (Beirau et al. 2010), sample E2335 exhibits anisotropic Raman spectra (see Fig. 3). As discussed above, anisotropic Raman scattering is typical of single-crystal solids, which unambiguously suggests that the structure of metamict titanite cannot be considered as quasi-amorphous. Neither it can be considered as polycrystalline, i.e., that the existing crystalline regions are almost coherent with respect to each other, regardless of the amorphous matter between the crystalline nanoregions. This result is in agreement with the TEM data, revealing an overall monocrystalline-type electron diffraction pattern as recorded from an individual particle and crystalline nanoregions, which are only slightly misaligned with respect each other. On the other hand, as in the case for heavily metamict titanite samples (M28173 and M28696), the orientation dependence of the Raman scattering of sample E2335 is more strongly pronounced than for crystalline pure titanine, as well as for slightly metamict titanite sample M28658. This indicates that the strong anisotropy of the Raman scattering of metamict titanete, especially in the range 600–800 cm^{-1}, is related to anisotropic structural damage. The profile of the Raman signal collected in the vicinity of 600 cm^{-1} (from heavily metamict titanite in orientation 1) resembles that of well-crystalline titanite. On the other hand, the profile collected in orientation 2 differs from the spectrum of well-crystalline titanite. The latter Raman peak is typical of TiO_6 stretching (Heyns et al. 2000; Su et al. 2000; Kostov-Kytin et al. 2005) and in orientation 1 it is slightly broadened and shifted toward lower wavenumbers with increasing degree of metamictization (~572 cm^{-1} for the most heavily metamict sample M28696). By contrast, the Raman scattering in orientation 2 near 600 cm^{-1} substantially broadens and the intensity maximum shifts toward higher wavenumbers with increase in the degree of metamictization (~650 cm^{-1} for the most heavily metamict sample M28696), approaching but not reaching the position of the band near 750 cm^{-1} in the spectrum of titanite glass. It should be noted that we have thoroughly checked the orientation dependence of the Raman scattering of pure single-crystal titanite and we did not observe a Raman spectrum in which the signal at 600 cm^{-1} is suppressed, while new signals near 570 or 650 cm^{-1} are enhanced. Thus, these spectral changes cannot be related to orientation effects of pure crystalline titanite but likely reflect the changes of the Ti-O bond stretching modes related to the radiation-induced structural damage. The decrease in the position of the peak near 600 cm^{-1} with degree of metamictization (as observed in orientation 1) is in full accordance with the radiation-induced enlargement of the unit-cell volume detected by XRD (Hawthorne et al. 1991), which indicates that the Raman scattering collected in orientation 1 mainly represents the structural state of the crystalline nanoregions.

The Ti^{4+} cations in amorphous Ti-Si-O frameworks can be 6-, 5-, and 4-coordinated (Alberto et al. 1995; Nasu et al. 1997; Henderson and Fleet 1995; Farges et al. 1996). Penta- and tetra-coordinated Ti^{4+} has been suggested to exist in heavily metamict titanite (Hawthorne et al. 1991; Farges et al. 1997; Zhang et al. 2002). The Ti-O bond strength increases with decreasing Ti coordination. Consequently, the resultant Ti-O bond stretch-

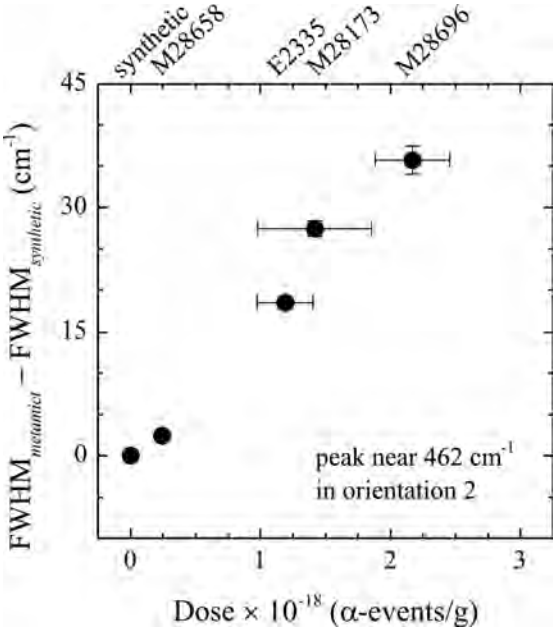

FIGURE 5. The deviation of the FWHM of the peak near 465 cm^{-1} measured in orientation 2 from the FWHM for synthetic titanite vs. the accumulated α-radiation dose (see Table 1). The error bars of the widths represent the uncertainties obtained from the spectrum-profile fittings.

ing mode in a disordered framework comprising octa-, penta-, and tetrahedrally coordinated Ti would be positioned at higher wavenumbers as compared to the Ti-O bond stretching mode in a framework that contains only TiO_6 octahedra. Thus, we propose that the metamictization-related spectral features observed in orientation 2 are also sensitive to radiation-induced amorphization involving a partial change in the Ti coordination and subsequent rearrangements of the Ti-O-Ti and Si-O-Ti linkages.

This suggestion is strongly supported by the local structural species responsible for the atomic vibrations giving rise to the Raman scattering in the two distinctive orientations. A close examination of the atomic arrangements of titanite (see Fig. 6) reveals that, in orientation 1, the polarization of the incident light $\mathbf{E}_i$ lies in a plane approximately perpendicular to the chains of TiO_6 octahedra, whereas in orientation 2, the vector $\mathbf{E}_i$ is in a plane approximately parallel to the TiO_6 chains. The interchain connectivity is realized by SiO_4-TiO_6 linkages forming four-membered polyhedral rings of SiO_4-TiO_6-SiO_4-TiO_6 as the two octahedra are from different TiO_6 chains. As can be seen in Figure 6, these 4-membered rings in orientation 1 are approximately in the same plane as $\mathbf{E}_i$ and therefore, peaks generated by ring "breathing" modes, involving in-plane vibrations of the SiO_4-TiO_6 bridging oxygen atoms, would be very sensitive to any connectivity and stacking faults in the periodic atomic framework. On the other hand, Ti-O stretching vibrations of oxygen atoms linking the TiO_6 octahedra in chains should generate strong Raman peaks in orientation 2. A plausible change in the Ti coordination would not only influence the interchain connectivity but would also induce broken TiO_6-TiO_6 linkages, i.e., loss of periodicity in all directions. Thus, the Raman scattering measured in orientation 2 is much more sensitive to the presence of radiation-induced amorphous regions than that collected in orientation 1.

Effect of annealing. To verify the possibility of separately studying the evolution of defects inside crystalline nanoregions and the amorphous-to-crystalline nanoscale transitions, we analyzed the Raman spectra of sample E2335 subjected to multistep annealing (Fig. 7). All spectra measured from annealed sample E2335 were effectively fitted using the same number of Lorent-

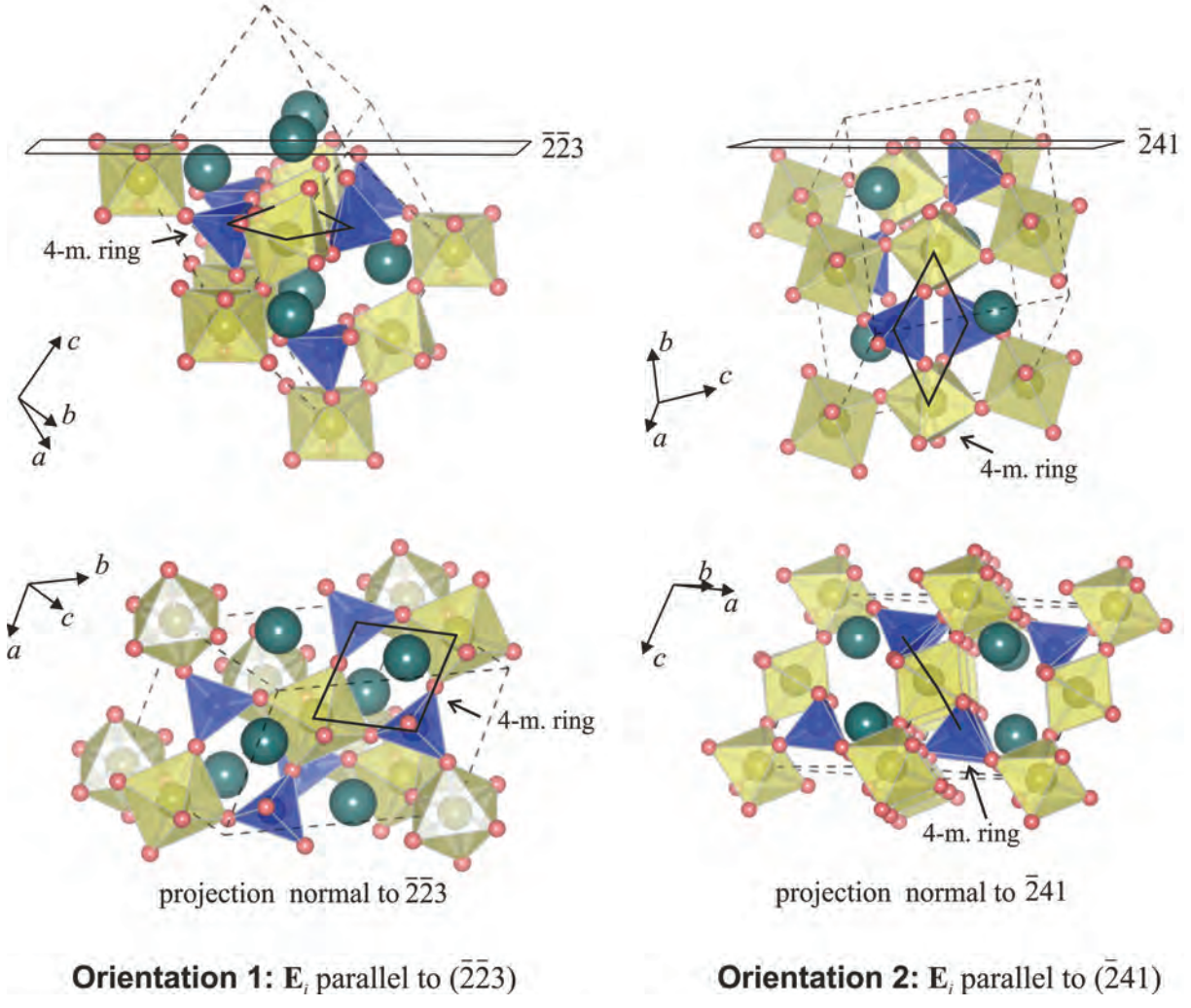

FIGURE 6. Projections of the titanite structure corresponding to orientations 1 (**left**) and 2 (**right**). The figure was prepared using the VESTA software package (Momma and Izumi 2008). (Color online.)

zian functions as for non-annealed sample E2335. In orientation 1, the position of the peak near 600 cm^{-1} arising from the Ti-O bond stretching increases with increasing annealing temperature T_{an} up to T_{an} ~900 K, then remains nearly constant (Fig. 8). At the same time, the FWHM of this peak generally decreases with increasing annealing temperature, as the trend is more pronounced at higher T_{an}. The peaks near 422 and 485 cm^{-1} measured in orientation 1, which are related to SiO_4 bending modes (Beirau et al. 2010), (see Fig. 9) as well as the external SiO_4 mode near 287 cm^{-1} (not shown), exhibit the same dependence on the annealing temperature. The dependence of the FWHM on T_{an} for the above-mentioned peaks indicates a gradual recovery of the structure, i.e., it is related to the suppression of defects and enlarged length of structural coherence in the crystalline regions. The saturation of the wavenumbers of the corresponding TiO_6 and SiO_4 phonon modes above T_{an} ~900 K indicates that further annealing leads to negligible improvement of the connectivity of the SiO_4-TiO_6-SiO_4-TiO_6 rings.

As expected, the T_{an}-dependencies of the peaks observed in orientation 2 differ from the trends measured in orientation 1. The Raman signal near 603 cm^{-1} generated by Ti-O bond stretching decreases in wavenumber with increasing T_{an} (see Fig. 10). This peak also shows an excess in the FWHM with a maximum near 750 K, indicating the occurrence of structural transformations. According to hard-mode spectroscopy (Salje and Bismayer 1997), a maximum of the FWHM of a Raman or infrared peak as a function of temperature (or any other thermodynamic variable characterizing the system under consideration) reflects the damping of the corresponding phonon mode when the system approaches a phase transition. In the case of metamict titanite subjected to annealing, the maximum of the FWHM as a function of T_{an} corresponds to the temperature at which the fraction of amorphous matter undergoing recrystallization is at a maximum. Thus, the spectral changes suggest that annealing leads to a recovery of the octahedral coordination of Ti atoms and consequent improvement of the Ti-O-Ti chain connectivity. The Raman peaks measured in orientation 2 that are related to O-Si-O bond bending vibrations (see Fig. 11) broaden between 650 and 950 K with a strong maximum of FWHMs vs. T_{an} near 750 K, which also reveals the occurrence of structural transformations. The positions of these two peaks remain unchanged up to T_{an} ~650 K, then strongly increase, and above ~900 K are constant. In addition, the lowest-energy mode (near 72 cm^{-1}) observed in orientation 2, which should be indicative of the overall atomic rearrangements, also shows a maximum of the FHWM near 750 K (Fig. 12). Thus, all annealing-induced spectral changes detected in orientation 2 unambiguously indicate that the system undergoes significant structural alteration, which we attribute to annealing-induced recrystallization of the preexisting amorphous nanoregions in metamict titanite. Annealing enhances the reappearance of 6-coordinated Ti in the non-crystalline regions and thus induces polyhedral linkages typical of crystalline titanite. Therefore, by changing the short- and the intermediate-range order, annealing drives the framework of the radiation-amorphized

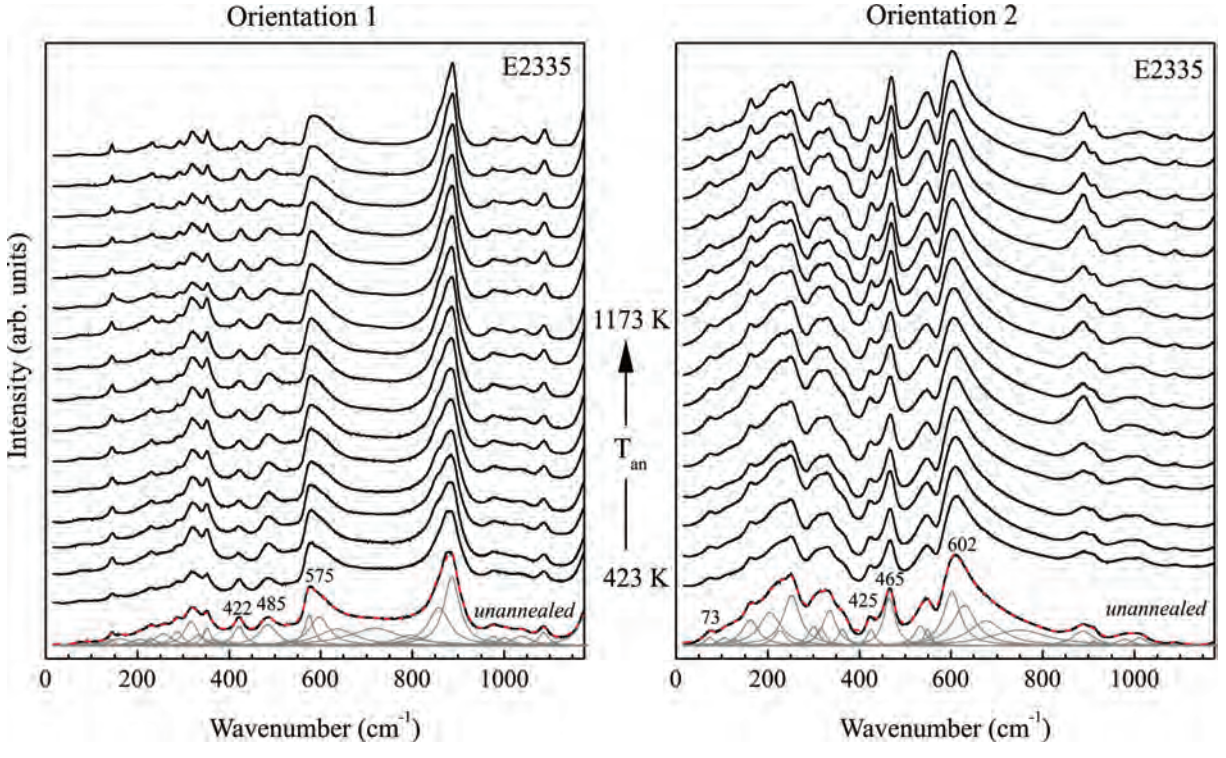

FIGURE 7. Raman spectra of sample E2335 measured in orientation 1 (**a**) and orientation 2 (**b**) before and after the multistep annealing at temperatures between 423–1173 K with 50 K step, annealing time at each step of 2 h. The thin gray lines represent the fitting Lorentzians to the spectra measured before annealing, the red dashed lines are the corresponding resultant spectral profiles. The wavenumbers of the peaks further discussed in the text are also given in the plots. (Color online.)

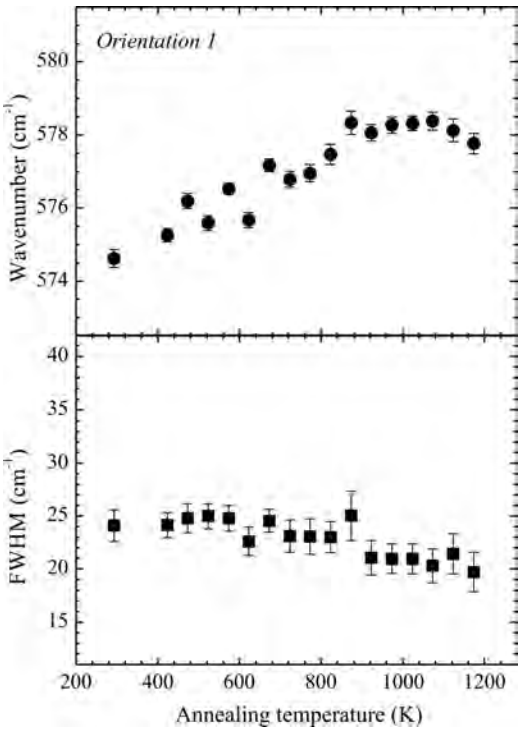

FIGURE 8. Wavenumber and FWHM vs. annealing temperature for the peak near 575 cm^{-1}, arising from Ti-O bond stretching, measured from sample E2335 in orientation 1. The error bars represent the uncertainties obtained from the spectrum-profile fittings.

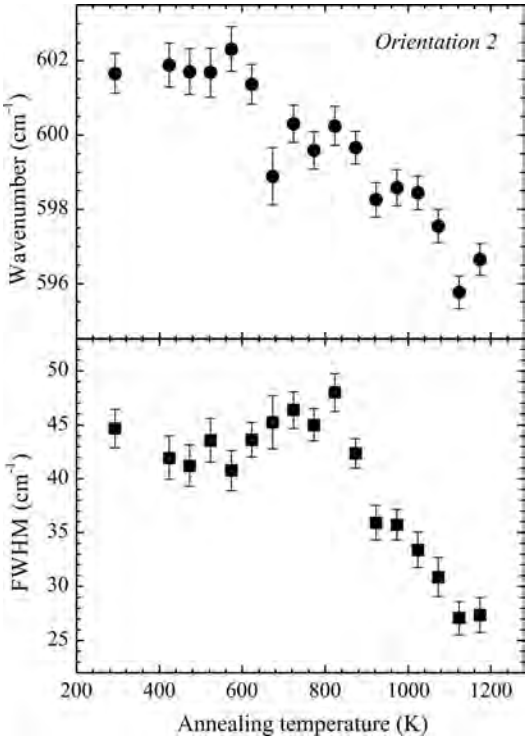

FIGURE 10. Wavenumber and FWHM vs. annealing temperature for the peak near 607 cm^{-1}, arising from Ti-O bond stretching, measured from sample E2335 in orientation 2. The error bars represent the uncertainties obtained from the spectrum-profile fittings.

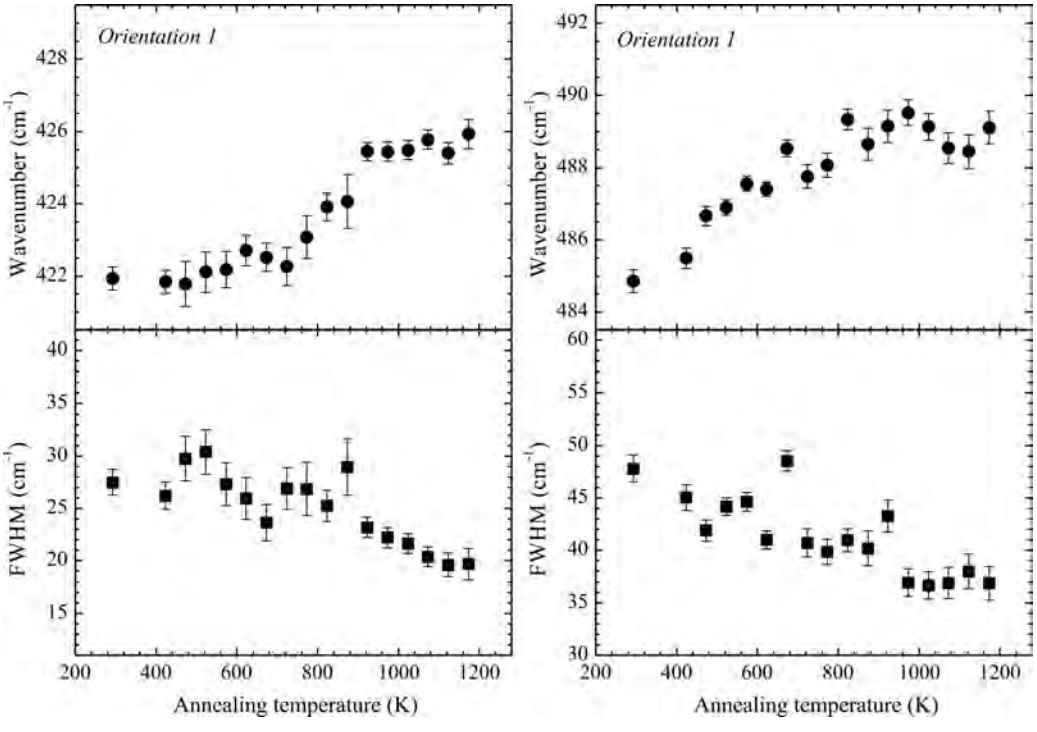

FIGURE 9. Wavenumber and FWHM vs. annealing temperature for the peaks near 422 and 485 cm^{-1} related to bond O-Si-O bending modes measured from sample E2335 in orientation 1. The error bars represent the uncertainties obtained from the spectrum-profile fittings.

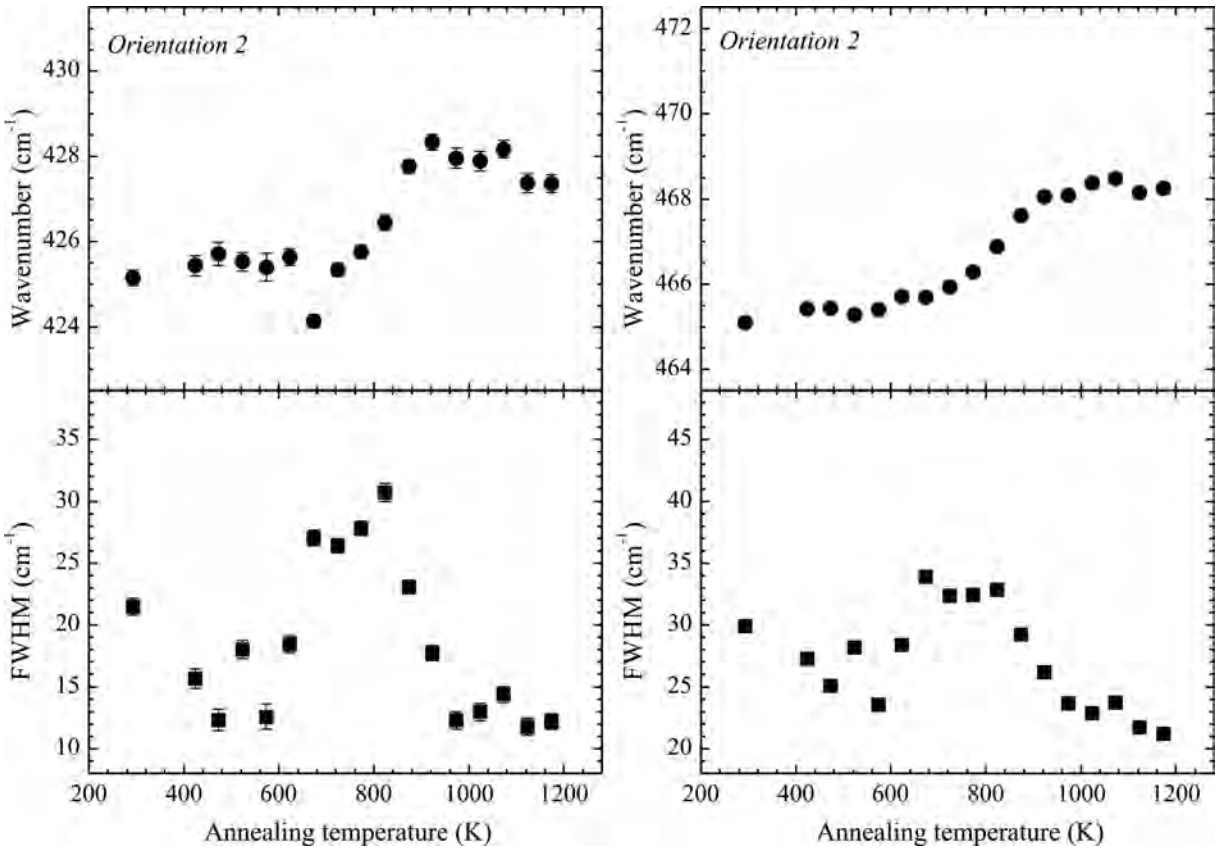

FIGURE 11. Wavenumber and FWHM vs. annealing temperature for the peaks near 422 and 485 cm^{-1} related to bond O-Si-O bending modes measured from sample E2335 in orientation 2. The error bars represent the uncertainties obtained from the spectrum-profile fittings.

parts to develop periodicity typical of titanite. The annealing-induced reduction of periodic faults and improved structural correlation in the crystalline nanoregions should facilitate the recrystallization of the amorphous nanoregions. Since the SiO_4 modes giving rise to Raman peaks in orientation 2 show significant excess of FWHM in the T_{an}-range 650–950 K, whereas the SiO_4 modes generating Raman peaks in orientation 1 do not, one can speculate that the intermediate-range order, namely Ti-O-Si linkages, within the planes normal to the TiO_6 chains is more or less preserved, which supports the process of structural recovery of titanite. However, the annealing of heavily metamict titanate (damage index ≥8) up to 1173 K for 2 h per step of 50 K cannot lead to a complete recrystallization of the global structure. The Raman spectral profiles of sample E2335 measured after the final annealing step performed in this study (see Fig. 7), clearly show that the titanite structure is only partially recovered and still heavily damaged.

CONCLUDING REMARKS

Orientation-dependent Raman spectroscopy of metamict titanite provides the unique opportunity to discriminately analyze the radiation-induced development of defects inside the crystalline nanoregions and crystalline-to-amorphous transformations in nanometer-sized regions as well as the corresponding annealing-induced reverse processes: temperature-driven suppression of defects in the crystalline nanoregions and recrystallization of the preexisting amorphous nanoregions.

The structural state of heavily metamict titanite is highly anisotropic, indicating coherence between the different crystalline regions. In this sense, the structure of metamict titanite consists of a crystalline matrix with high degree of periodic faults and abundant amorphous nanoregions embedded in the matrix. The radiation-induced periodic faults in the crystalline substance are related to the disturbance of SiO_4-TiO_6-SiO_4-TiO_6 rings comprising TiO_6 octahedra from different chains. The radiation-induced amorphization is related to the partial change of Ti coordination from octahedral to pyramidal and/or tetrahedral, which in turn violates the Ti-O-Ti intrachain linkages. This indicates that the affinity of the structure as a whole to accumulate radiation-induced defects, which leads to the development of amorphous regions, is different in the different crystallographic planes of titanite. The plane containing Si-O-Ti-O bond closed contours is less susceptible to a self-accumulation of defects as compared to the perpendicular plane, which contains chains of Ti-O bonds.

Multistep annealing by 50 K for 2 h per step gradually suppresses the structural defects in the crystalline substance as the improvement of the SiO_4-TiO_6 connectivity within planes near

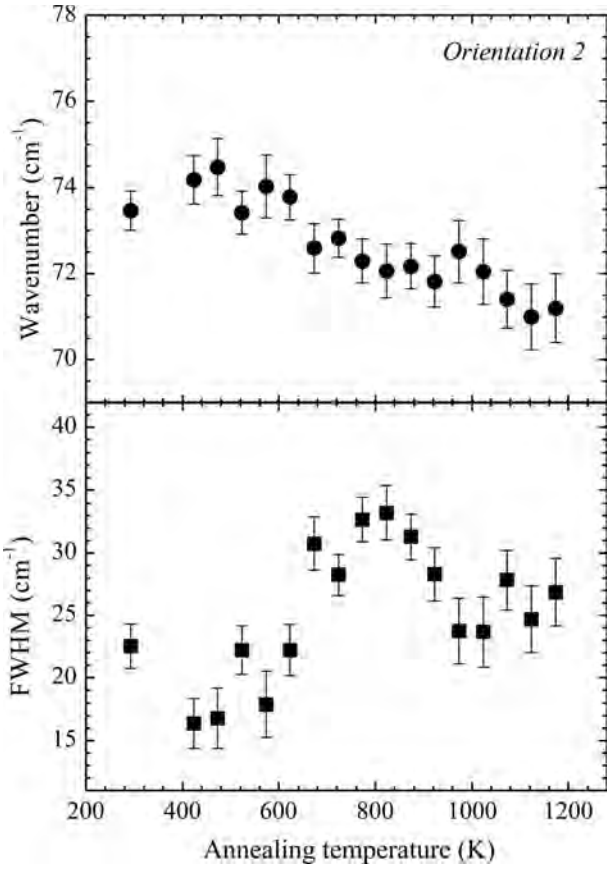

FIGURE 12. Wavenumber and FWHM vs. annealing temperature for the lowest-energy peak near 73 cm^{-1} measured from sample E2335 in orientation 2. The error bars represent the uncertainties obtained from the spectrum-profile fittings.

perpendicular to the TiO_6 chains reaches saturation at ~900 K. The annealing-induced recrystallization of the radiation-induced amorphous nanoregions begins at ~650 K, the process is most intense near 750 K, and considerably weakens above 950 K. Raman scattering shows that annealing up to 1173 K is insufficient to recover the crystalline structure of the studied metamict titanite sample, which is in full accordance with the results obtained by resonance ultrasound spectroscopy (Salje et al. 2011b).

ACKNOWLEDGMENTS

Financial support by the Deutsche Forschungsgemeinschaft (BI 374/9-1, INST-152/460-1) is gratefully acknowledged.

REFERENCES CITED

Alberto, H.V., de Campos, N.A., and Mysen, B.O. (1995) The structural role of titanium in silicate glasses—A Raman-study of the system CaO-SiO_2-TiO_2. Physics and Chemistry of Glasses, 36, 114–122.

Beirau, T., Bismayer, U., Mihailova, B., Paulmann, C., and Groat, L. (2010) Structural phenomena of metamict titanite: a synchrotron, X-ray diffraction and vibrational spectroscopic study. Phase Transitions, 83, 694–702.

Chrosch, J., Bismayer, U., and Salje, E.K.H. (1997) Anti-phase boundaries and phase transitions in titanite: An X-ray diffraction study. American Mineralogist, 82, 677–681.

Chrosch, J., Colombo, M., Malcherek, T., Salje, E.K.H., Groat, L.A., and Bismayer, U. (1998) Thermal annealing of radiation damaged titanite. American Mineralogist, 83, 1083–1091.

Ewing, R.C. (2007a) Ceramic matrices for plutonium disposition. Progress in Nuclear Energy, 49, 635–643.

——— (2007b) Displaced by radiation. Nature, 445, 161–162.

Ewing, R.C., Chakoumakos, B.C., Lumpkin, G.R., Murakami, T., Greegor, R.B., and Lytle, F.W. (1988) Metamict minerals: Natural analogues for radiation damage effects in ceramic nuclear waste forms. Nuclear Instruments and Methods in Physics Research, B, 32, 487–497.

Farges, F. (1997) Fivefold-coordinated Ti^{4+} in metamict zirconolite and titanite: A new occurrence shown by Ti K-edge XANES spectroscopy. American Mineralogist, 82, 44–50.

Farges, F., Brown, G.E. Jr., Navrotsky, A., Gan, H., and Rehr, J.R. (1996) Coordination chemistry of Ti(IV) in silicate glasses and melts: III. Glasses and melts from ambient to high temperatures. Geochimica et Cosmochimica Acta, 60, 3055–3065.

Farnan, I., Cho, H., and Weber, W.J. (2007) Quantification of actinide α-radiation damage in minerals and ceramics. Nature, 445, 190–193.

Geisler, T. and Pidgeon, R.T. (2002) Raman scattering from metamict zircon: comments on ‘‘Metamictisation of natural zircon: accumulation versus thermal annealing of radioactivity-induced damage″ by Nasdala et al. Contributions to Mineralogy and Petrology, 143, 750–755.

Hawthorne, F.C., Groat, L.A., Raudsepp, M., Ball, N.A., Kimata, M., Spike, F., Gaba, R., Halden, N.M., Lumpkin, G.R., Ewing, R.C., and others. (1991) Alpha-decay damage in titanite. American Mineralogist, 76, 370–396.

Henderson, G.S. and Fleet, M.E. (1995) The structure of Ti silicate glasses by micro-Raman spectroscopy. The Canadian Mineralogist, 33, 399–408.

Heyns, A.M., Harden, P.M., and Prinsloo, L.C. (2000) Resonance Raman study of the high-pressure phase transition in chromium-doped titanite, $CaTiOSiO_4$. Journal of Raman Spectroscopy, 31, 837–841.

Higgins, J.B. and Ribbe, P.H. (1976) The crystal chemistry and space groups of natural and synthetic titanites. American Mineralogist, 61, 878–888.

Kek, S., Aroyo, M., Bismayer, U., Schmidt, C., Eichhorn, K., and Krane, H.G. (1997) The two-step phase transition of titanite, $CaTiSiO_5$: a synchrotron radiation study. Zeitschrift für Kristallographie, 212, 9–19.

Kostov-Kytin, V., Mihailova, B., Kalvachev, Yu., and Tarassov, M. (2005) Atomic arrangements in amorphous sodium titanosilicate precursor powders. Microporous and Mesoporous Materials, 86, 223–230.

Kroumova, E., Aroyo, M.I., Perez-Mato, J.M., Kirovm, A., Capillas, C., Ivantchev, S., and Wondratschek, H. (2003) Bilbao Crystallographic Server: Useful Databases and Tools for Phase-Transition Studies. Phase Transitions, 76, 155–170.

Lumpkin, G.R., Eby, R.K., and Ewing, R.C. (1991) Alpha-recoil damage in titanite ($CaTiSiO_5$): Direct observation and annealing study using high resolution transmission electron microscopy. Journal of Materials Research, 6, 560–564.

Malcherek, T., Domeneghetti, C.M., Tazzoli, V., Salje, E.K.H., and Bismayer, U. (1999) A high temperature diffraction study of synthetic titanite $CaTiOSiO_4$. Phase Transitions, 69, 119–131.

Malcherek, T., Paulmann, C., Domeneghetti, M.C., and Bismayer, U. (2001) Diffuse scattering anisotropy and the $P2_1/a$–$A2/a$ phase transition in titanite, $CaTiOSiO_4$. Journal of Applied Crystallography, 34, 108–113.

Momma, K. and Izumi, F. (2008) VESTA: a three-dimensional visualization system for electronic and structural analysis. Journal of Applied Crystallography, 41, 653–658.

Muller, I. and Weber, W.J. (2001) Plutonium in crystalline ceramics and glasses. MRS Bulletin, 26, 698–706.

Nasdala, L., Wenzel, M., Vavra, G., Irmer, G., Wenzel, T., and Kober, B. (2001) Metamictization of natural zircon: accumulation versus thermal annealing of radioactivity-induced damage. Contributions to Mineralogy and Petrology, 141, 125–144.

Nasu, H., Kurachi, K., Mito, A., Matsuoka, J., and Kamiya, K. (1997) Second harmonic generation and structure of mixed alkali titanosilicate glasses. Journal of Non-Crystalline Solids, 217, 182–188.

Otwinowski, Z. and Minor, W. (1997) Processing of X-ray diffraction data collected in oscillation mode. Methods in Enzymology, 276, 307–326.

Paulmann, C., Bismayer, U., and Groat, L.A. (2000) Thermal annealing of metamict titanite: A synchrotron radiation and optical birefringence study. Zeitschrift für Kristallographie, 215, 678–682.

Salje, E.K.H. and Bismayer, U. (1997) Hard mode spectroscopy: The concept and applications. Phase Transitions, 63, 1–75.

Salje, E.K.H., Safarik, D.J., Taylor, R.D., Pasternak, M.P., Modic, K.A., Groat, L.A. and Lashley, J.C. (2011a) Determination of iron sites and the amount of amorphization in radiation-damaged titanite ($CaSiTiO_5$). Journal of Physics: Condensed Matter, 23, 105402 (3 p).

Salje, E.K.H., Safarik, D.J., Lashley, J.C., Groat, L.A., and Bismayer, U. (2011b) Elastic softening of metamict titanite $CaTiSiO_5$: Radiation damage and annealing. American Mineralogist, 96, 1254–1261.

Salje, E.K.H., Taylor, R.D., Safarik, D.J., Lashley, J.C., Groat, L.A., Bismayer, U., Evans, R.J., and Friedman, R. (2012) Evidence for direct impact damage in metamict titanite $CaTiSiO_5$. Journal of Physics: Condensed Matter, 24, 052202 (5 p).

Speer, J.A. and Gibbs, G.V. (1976) The crystal structure of synthetic titanite, $CaTiOSiO_4$, and the domain texture of natural titanites. American Mineralogist, 61, 238–247.

Su, Y., Balmer, M.L., and Bunker, B.C. (2000) Raman spectroscopic studies of silicotitanates. Journal of Physical Chemistry B, 104, 8160–8169.

Taylor, M. and Brown, G.E. (1976) High-temperature structural study of the $P2_1/a \leftrightarrow A2/a$ phase transition in synthetic titanite, $CaTiSiO_5$. American Mineralogist, 61, 435–447.

Tucker, R.D., Ashwal, L.D., Handke, M.J., Hamilton, M.A., Le Grange, M., and Rambeloson, R.A. (1999) U-Pb geochronology and isotope geochemistry of the Archean and Proterozoic rocks of North-Central Madagascar. Journal of Geology, 107, 135–153.

Vance, E.R. and Metson, J.B. (1985) Radiation damage in natural titanites. Physics and Chemistry of Minerals, 12, 255–260.

Weber, W.J., Ewing, R.C., Angell, C.A., Arnold, G.W., Cormack, A.N., Delaye, J.M., Griscom, D.L., Hobbs, L.W., Navrotsky, A., Price, D.L., Stoneham, A.M., and Weinberg, M.C. (1997) Radiation effects in glasses used for immobilization of high-level waste and plutonium disposition. Journal of Materials Research, 12, 1948–1978.

Weber, W.J., Ewing, R.C., Catlow, C.R.A., Diaz de la Rubia, T., Hobbs, L.W., Kinoshita, C., Matzke, Hj., Motta, A.T., Nastasi, M., Salje, E.K.H., Vance, E.R., and Zinkle, S.J. (1998) Radiation effects in crystalline ceramics for the immobilization of high-level nuclear waste and plutonium. Journal of Materials Research, 13, 1434–1484.

Zhang, M., Salje, E.K.H., Bismayer, U., Unruh, H.-G., Wruck, B., and Schmidt, C. (1995) Phase transition(s) in titanite $CaTiSiO_5$: An infrared spectroscopic, dielectric response and heat capacity study. Physics and Chemistry of Minerals, 22, 41–49.

Zhang, M., Salje, E.K.H., and Bismayer, U. (1997) Structural phase transition near 825 K in titanite: Evidence from infrared spectroscopic observations. American Mineralogist, 82, 30–35.

Zhang, M., Salje, E.K.H., Bismayer, U., Groat, L.A., and Malcherek, T. (2002) Metamictization and recrystallization of titanite: An infrared spectroscopic study. American Mineralogist, 87, 882–890.

Manuscript received October 10, 2011
Manuscript accepted April 27, 2012
Manuscript handled by Grant Henderson